

Supplementary information:

Limiting optical diodes enabled by the phase transition of vanadium dioxide

Chenghao Wan^{1,2}, Erik Horak³, Jonathan King^{1,4}, Jad Salman¹, Zhen Zhang⁵, You Zhou⁶, Patrick Roney¹,
Bradley Gundlach¹, Shriram Ramanathan⁵, Randall Goldsmith³, Mikhail A. Kats^{1,2,7}

¹ Department of Electrical and Computer Engineering, University of Wisconsin-Madison, Madison, Wisconsin 53706, USA

² Department of Materials Science & Engineering, University of Wisconsin-Madison, Madison, Wisconsin 53706, USA

³ Department of Chemistry, University of Wisconsin-Madison, Madison, Wisconsin 53706, USA

⁴ Power Services Group, JENSEN HUGHES, Oakbrook Terrace, IL 60181, USA

⁵ School of Materials Engineering, Purdue University, West Lafayette, IN 47907, USA

⁶ Harvard John A. Paulson School of Engineering and Applied Sciences, Harvard University, Cambridge, MA 02138, USA

⁷ Department of Physics, University of Wisconsin-Madison, Madison, Wisconsin 53706, USA

Section 1. Optimization of forward transmission and absorption asymmetry ratio

To balance between the two figures of merit (maximized absorption asymmetry ratio and transmission in the low-power state), we swept the thicknesses of Au and VO₂ and calculated the transmission and asymmetry ratio of absorption using the transfer-matrix method, as shown in Fig. S-1. The same *c*-plane sapphire substrate was used in all calculations. Thicker VO₂ and Au generally results in larger absorption asymmetry, but also lower transmission (Fig. S-1(a)). We chose to fabricate a sample with 100 nm VO₂ and 10 nm Au, resulting in transmission of ~ 0.22 at low power, and a six-fold absorption asymmetry ratio (absorption = 0.11 for forward propagation, and 0.67 for backward propagation).

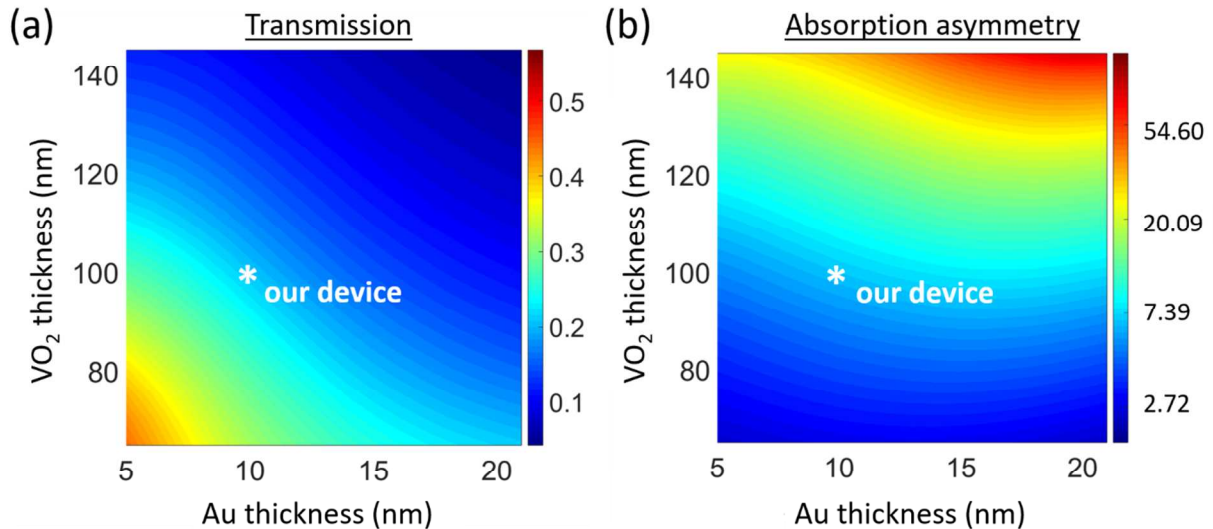


Figure S-1. (a) Transmission and (b) absorption-asymmetry ratio ($A_{backward}/A_{forward}$) of our thin-film device with the thickness of VO₂ varying from 60 to 150 nm, and the thickness of Au varying from 5 to 21 nm. The refractive index of VO₂ used in these calculations corresponds to its insulating phase.

Section 2. SEM and AFM characterization of our sputtered VO₂ film on c-plane sapphire

To examine the surface uniformity of the VO₂, we characterized the post-growth film using an SEM (Zeiss LEO 1530) and an AFM (Veeco MultiMode SPM) in tapping mode (Fig. S-2). Based on five AFM images, each of which is 10 μm by 10 μm (*e.g.*, Fig. S-2(b)), we calculated the surface roughness to be $R_a = 4.11$ nm.

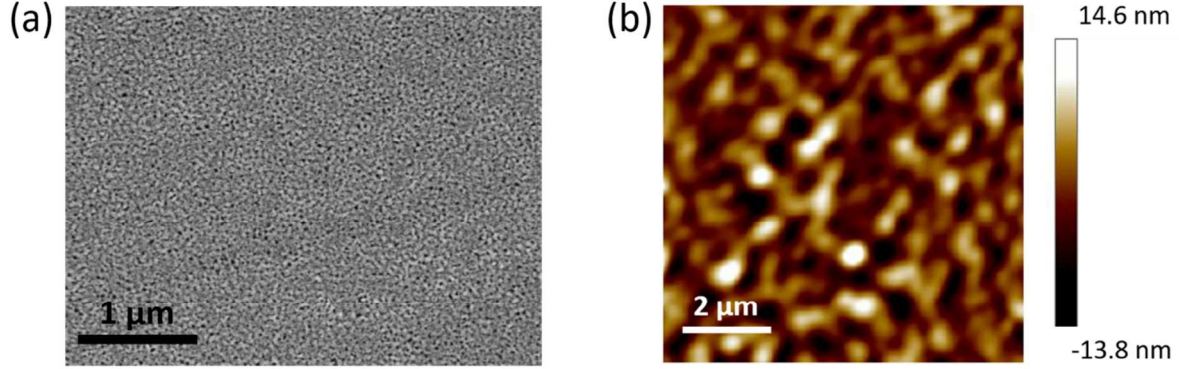


Figure S-2. (a) SEM and (b) AFM images of post-growth 100 nm VO₂ on a c-plane sapphire substrate. A surface roughness $R_a = 4.11$ nm was calculated based on five AFM images, each of which is 10 μm by 10 μm.

Section 3. Details of our model

Spectroscopic ellipsometry (SE) was used to extract the complex refractive indices of VO₂ in the insulating (30 °C) and metallic phase (90 °C), for free-space wavelengths from 200 nm to 2000 nm. In our fitting model, optical constants of VO₂ are described by a general oscillator (GNO) function [S1], which includes five Gaussian oscillators [S2] for the insulating phase, and an additional Drude term [S2] for the metallic phase. The results are shown in Fig. 1(b) in the main text. An effective medium approximation (Looyenga mixing rule; Eq. (S1)) [S3][S4] was then used to estimate the refractive indices of VO₂ across its phase transition, as shown in Fig. S-3(a).

$$\tilde{\epsilon}_{eff}^m = (1 - f)\tilde{\epsilon}_{insulating}^m + f\tilde{\epsilon}_{metallic}^m \quad (S1)$$

$$\tilde{n} = n + i\kappa = \sqrt{\tilde{\epsilon}} \quad (S2),$$

where $\tilde{\epsilon}$ is the complex dielectric function of VO₂, f is the metallic fraction, and m is an exponent that describes the anisotropy of the material. f and m were both estimated using the same method as in Ref. [S4]. The effective optical refractive index was then calculated using Eq. (S2). For our experimental wavelength ($\lambda = 1.32$ μm), there is a significant change in the complex refractive index of VO₂, from $\tilde{n} =$

$3.2 + 0.6i$ to $\tilde{n} = 1.7 + 2.4i$ across its phase transition. The temperature-dependent refractive index of VO₂ (Fig. S-3(a)) enabled us to calculate the absorption within our device for both forward and backward incidence as a function of temperature (Fig. S-3(b)). These absorption curves were used as input parameters for our COMSOL heat-transfer model.

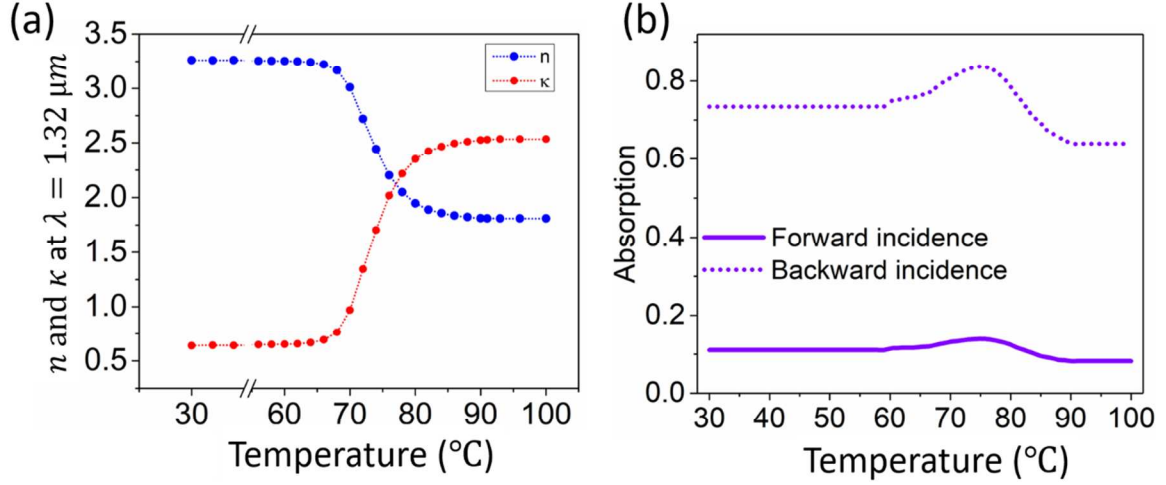


Figure S-3. (a) Calculated refractive index of VO₂ (at $\lambda = 1.32 \mu\text{m}$) from $T = 30$ to $100 \text{ }^\circ\text{C}$, using the Looyenga mixing rule. (b) Calculated combined absorption in the VO₂ and Au layers (region 1 and 3 in Fig. 2(c)) as a function of the bias temperature.

In our heat-transfer model, the temperature evolution of the structure follows the general steady-state heat equation (Eq. (S3)) [S5], by which the generated heat (Q) is proportional to the local heat-flux density (\mathbf{q}):

$$-\nabla \cdot \mathbf{q} + Q(r, z, T) = 0 \quad (\text{S3}),$$

where

$$\mathbf{q} = -k\nabla T(r, z) \quad (\text{S4})$$

$$Q(r, z, T) = A(T(r, z)) \quad (\text{S5})$$

Eq. (S4) is Fourier's law, which describes that the heat-flux density is proportional to the gradient of temperature (T), where k is the thermal conductivity. Eq. (S5) assumes that the heat-generation term (Q) is based on the amount of laser power absorbed in each layer (A). The absorption within the VO₂ layer is a function of the varying local temperature at each spatial position (r, z), and is given in Fig. S-3(b).

Section 4. Proof-of-concept design using VO₂ with a narrower phase transition

The relatively broad temperature range of the transition of the VO₂ films used in our experiments is a potential limitation of our device. For the maximum laser intensity we could experimentally achieve, there was no bias temperature for which the diode is maximally asymmetric; *i.e.*, the transmission is maximal for light incident from one side, and minimal for light incident from the other side. To realize maximal transmission asymmetry at the intensities in our experiment, one could use VO₂ with a narrower phase transition, *e.g.*, using other substrates or engineered strain conditions for oriented growth [S6][S7]. For comparison, the solid-point curve in Fig. S-4(a) is the calculated temperature-dependent transmission, generated based on Ref. [S6], assuming that the material has the same range of optical properties as that used in our work, but with a narrower phase-transition range (~6 °C, from 65 °C to 71 °C). The open-point curve in Fig. S-4(a) is the temperature-dependent transmission of our fabricated device. We used our model to investigate the diode performance of both designs. As shown in Fig. S-4(b), our simulation indicates that the design based on narrower-transition VO₂ can reach maximal transmission asymmetry when it is thermally biased between 55 and 63 °C, for the incident intensities described in the main text.

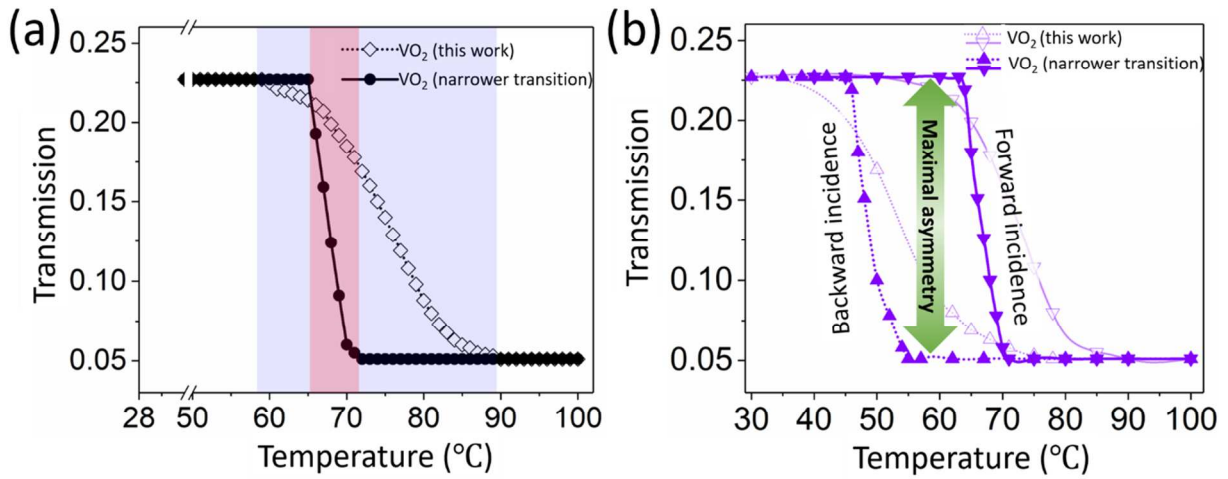


Figure S-4. (a) Temperature-dependent (during heating) transmission at $\lambda = 1.32 \mu\text{m}$ of our fabricated limiting optical diode, and calculated transmission of the same structure but using the VO₂ from Ref. [S6], assuming it has the same optical properties as our sputtered VO₂ but with a narrower phase transition. (b) Limiting diode performance simulated using our model, given the experimental conditions described in the main text. Duplicate of Fig. 3(b) in the main text.

Furthermore, our simulations show that our fabricated device—without any modification—will reach maximal asymmetry if driven at higher intensities than those realized in our experiment (Fig. S-5(a)). We calculated the intensity-dependent transmission-asymmetry ratio for a thermal-bias temperature at 50 °C, assuming both broader- and narrower-transition VO₂ in our limiting diodes. We also investigated the

performance at different bias temperatures (Fig. S-5(b)). Note that in Fig. S-5(b), we only show the results for the design based on narrower-transition VO₂. As expected, higher incident intensities are needed to trigger the device given lower bias temperatures. If the incident intensity is high enough, our design can work passively without any thermal bias.

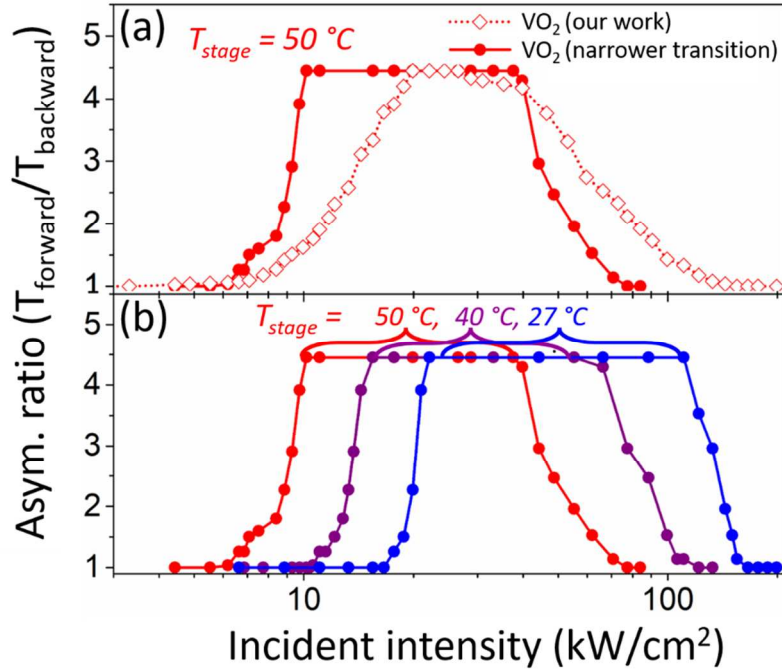


Figure S-5. Simulated transmission asymmetry ratio at varying incident intensities. **(a)** At $T_{\text{stage}} = 50\text{ }^\circ\text{C}$, comparison of the asymmetry ratio between identical devices based on narrower-transition VO₂ and the VO₂ used in our experiments. VO₂ with a narrower transition range enables a broader intensity range at which the asymmetry ratio is maximized. **(b)** Intensity-dependent asymmetry ratio of the design based on narrower-transition VO₂ at $T_{\text{stage}} = 27\text{ }^\circ\text{C}$, $40\text{ }^\circ\text{C}$, and $50\text{ }^\circ\text{C}$.

Section 5. Hysteresis discussion

In practice, one needs to consider the hysteresis effect in VO₂, as shown in Fig. S-6(a) for narrower-transition VO₂ from Ref. [S6], and Fig. S-6(c) for the VO₂ used in our experiments. To ensure that the diode is automatically reset when the illumination is turned off, one needs to set the bias temperature below the hysteresis region for the unilluminated diode. As identified using red shading in Fig. S-6(a), suitable thermal-bias temperatures range from room temperature to $56\text{ }^\circ\text{C}$ for the design based on narrower-transition VO₂. Given an input intensity of $6\text{ kW}/\text{cm}^2$ (the same simulation condition as in Fig. S-4(b)), one can achieve maximal asymmetry at bias temperatures from $55\text{ }^\circ\text{C}$ to $64\text{ }^\circ\text{C}$ (identified using green shading in Fig. S-6(b)). The region in common, where the green and red overlap, is the optimal

operating range of the device. (Fig. S-6(a, b)). For our fabricated device (Fig. S-6(c), (d)) given the same incident intensity, there are also suitable bias temperatures (identified using red shading in Fig. S-6(c)) at which asymmetric transmission can be realized, though the asymmetry ratio is not maximal. As our model predicts (Section 4), a higher incident intensity is necessary for our fabricated device to realize maximal asymmetry.

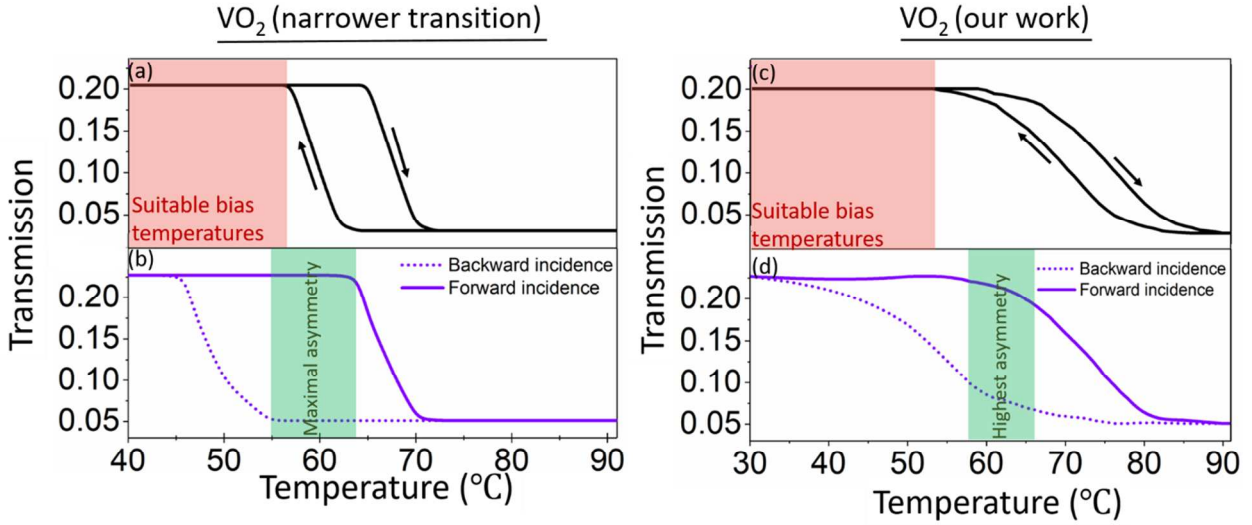


Figure S-6. (a) Hysteresis loop in the transmission of the device based on narrower-transition VO₂. The plot was generated using the same model as in Section 4, assuming no illumination. Temperatures within the red-shaded region are suitable to fully avoid device hysteresis. (b) Simulation results for the same diode design based on narrower-transition VO₂ for the high-power-incidence case (6 kW/cm², the same scenario as in Fig. S-4(b)). Temperatures within the green-shaded region yield maximal transmission asymmetry. (c) and (d) are the corresponding calculations for the design based on the VO₂ used in our experiments.

Section 6. Proof-of-concept design using a frequency selective surfaces (FSS)

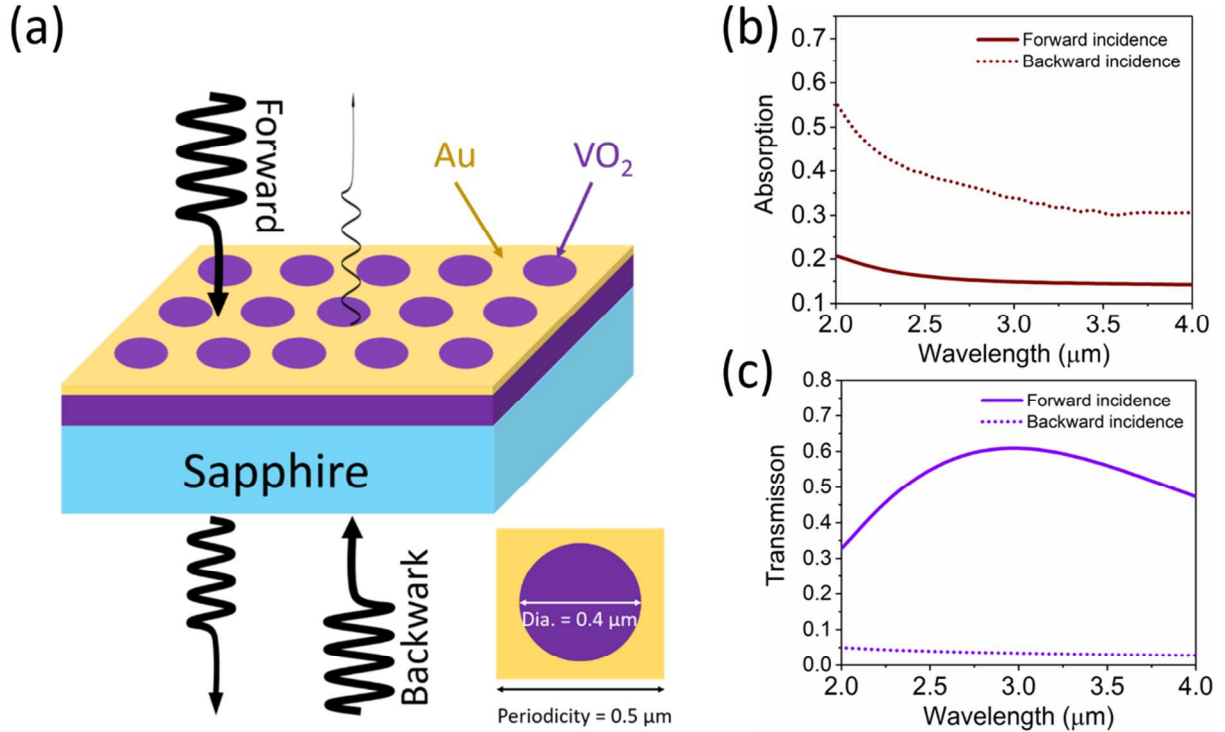


Figure S-7. (a) Design of a limiting optical diode based on a frequency selective surface (FSS), optimized using FDTD to feature a transmission maximum at $\lambda = 3 \mu\text{m}$, with an absorption asymmetry ratio of ~ 2 . **(b)** Simulated absorption within the device for both forward and backward incidences. **(c)** Simulated transmission spectra VO₂ in the insulating phase VO₂ in the metallic phase. For a certain range of incident powers, this will correspond to forward and backward incidence, respectively.

At low power, the low-power reciprocal transmission of the device experimentally demonstrated in the main text is ~ 0.22 , which may not be sufficient for certain applications. To show, in principle, that this figure of merit can be improved, we explored an alternate design based on frequency selective surface (FSS)^{8,9}. The design is shown in Fig. S-7, and comprises a 100-nm layer of VO₂ and a gold FSS with thickness of 55 nm, and circular apertures with a diameter of 400 nm in a square array with periodicity of 500 nm. The substrate is sapphire, like in the device in the main text.

At wavelengths around 3 μm (scalable by changing the size of the apertures), this design features a high transmission of ~ 0.6 when the VO₂ is in its insulating phase, and a low transmission of ~ 0.03 when the VO₂ for the metallic phase (Fig. S-7(c)). Like for the device in the main text, the asymmetry in absorption (Fig. S-7(b)) enables diode behavior based on selective triggering of the transition. With ideal operation, a transmission asymmetry ratio of ~ 20 can be reached at $\lambda = 3 \mu\text{m}$, with a low-power reciprocal transmission of above 0.6. We note that since we utilize the optical absorption in VO₂ to achieve diode

behavior, it is not possible to achieve a low-power transmission of 1 using our approach. We note, however, that VO₂ can also be triggered athermally using strong optical fields¹⁰, and it may be possible to use VO₂ as a component of a low-loss diode in a wavelength range where the intrinsic loss of the dielectric phase is relatively low.

References

- (S1) Herzinger, C. M.; Snyder, P. G.; Celii, F. G.; Kao, Y. □C.; Chow, D.; Johs, B.; Woollam, J. A. Studies of Thin Strained InAs, AlAs, and AlSb Layers by Spectroscopic Ellipsometry. *Journal of Applied Physics* **1996**, *79* (5).
- (S2) Johs, B.; Woollam, J. A.; Herzinger, C. M.; Hilfiker, J. N.; Synowicki, R. A.; Bungay, C. L. Overview of Variable-Angle Spectroscopic Ellipsometry (VASE): II. Advanced Applications; International Society for Optics and Photonics, 1999; Vol. 10294, p 1029404.
- (S3) Maron, N.; Maron, O. Criteria for Mixing Rules Application for Inhomogeneous Astrophysical Grains. *Monthly Notices of the Royal Astronomical Society* **2008**, *391* (2), 738–764.
- (S4) Rensberg, J.; Zhang, S.; Zhou, Y.; McLeod, A. S.; Schwarz, C.; Goldflam, M.; Liu, M.; Kerbusch, J.; Nawrodt, R.; Ramanathan, S.; et al. Active Optical Metasurfaces Based on Defect-Engineered Phase-Transition Materials. *Nano Letters* **2016**, *16* (2), 1050–1055.
- (S5) Cannon, J. R. *The One-Dimensional Heat Equation*; Addison-Wesley Pub. Co, 1984.
- (S6) Zhang, H.-T.; Zhang, L.; Mukherjee, D.; Zheng, Y.-X.; Haislmaier, R. C.; Alem, N.; Engel-Herbert, R. Wafer-Scale Growth of VO₂ Thin Films Using a Combinatorial Approach. *Nature Communications* **2015**, *6* (May), 8475.
- (S7) Ruzmetov, D.; Zawilski, K. T.; Narayanamurti, V.; Ramanathan, S. Structure-Functional Property Relationships in Rf-Sputtered Vanadium Dioxide Thin Films. *Journal of Applied Physics* **2007**, *102* (11), 113715.
- (S8) Munk, B. (Benedikt A. .; John Wiley & Sons. *Frequency Selective Surfaces : Theory and Design*; John Wiley, 2000.
- (S9) Mitra, R.; Chan, C. H.; Cwik, T. Techniques for Analyzing Frequency Selective Surfaces-a Review. *Proceedings of the IEEE* **1988**, *76* (12), 1593–1615.
- (S10) Pashkin, A.; Kübler, C.; Ehrke, H.; Lopez, R.; Halabica, A.; Haglund, R. F.; Huber, R.; Leitenstorfer, A. Ultrafast Insulator-Metal Phase Transition in VO₂ Studied by Multiterahertz Spectroscopy. *Physical Review B* **2011**, *83* (19), 195120.